J Solid State Electrochem (2009) 13:583–590
DOI 10.1007/s10008-008-0689-x

ORIGINAL PAPER

Local electron transfer rate measurements on modified and unmodified glassy carbon electrodes

Robert C. Tenent · David O. Wipf

Received: 1 August 2008 / Revised: 21 September 2008 / Accepted: 23 September 2008 / Published online: 8 October 2008

Abstract A natural and artificial distribution of electron transfer activity on glassy carbon electrodes can be observed and quantified by the use of scanning electrochemical microscopy (SECM). A large (sevenfold) spread in rate constant is found for randomly sampled sites on polished, untreated glassy carbon surfaces. Direct-mode oxidation with the SECM tip was used to produce small regions of oxidized carbon on a polished surface. A large increase in electron transfer rate for the Fe(II/III) ion is observed on the locally oxidized carbon surface in comparison to the unoxidized region. Rate constant measurements made along a line profiles the transition from unoxidized to oxidized surfaces. SECM images of defect sites show reaction–rate variations. Rate constants measured at several locations of the defective surface allows discrimination between the kinetic and topographic components of the SECM image.

Keywords Carbon electrode · Glassy carbon · Scanning electrochemical microscopy · Iron · Carbon oxides

Dedicated to the 80th birthday of Keith B. Oldham

R. C. Tenent · D. O. Wipf (✉)
Department of Chemistry, Mississippi State University,
310 Presidents Circle,
Mississippi State, MS 39762, USA
e-mail: wipf@ra.msstate.edu

Present address:
R. C. Tenent
National Renewable Energy Laboratory,
1617 Cole Boulevard,
Golden, CO 80401, USA

Introduction

A continuing topic of interest is the relationship between electrochemical performance of carbon electrodes and variations in surface microstructure [1–3]. More recent use of carbon structures for nanotechnology, such as carbon nanotubes and graphene sheets, has reemphasized the need to understand the relationship between interfacial structure and electrochemical reactivity [3, 4]. The structure of glassy carbon has been known for some time [5, 6] and has been shown to lead to variations in local electrode surface structure [7]. This is due to differences in exposed basal plane carbon where the carbon ring structure is in the plane of the electrode surface versus edge plane carbon where the carbon ring structure is not in the plane of the electrode surface. It has long been hypothesized that edge plane carbon sites are more active to electron transfer (ET) than basal plane sites and several groups have studied these variations [8–12].

This work presents the use of the scanning electrochemical microscope (SECM) to make direct measurements of variations in ET kinetics on glassy carbon electrode (GCE) surfaces. Conventional kinetic measurements, such as cyclic voltammetry (CV) and rotating disk voltammetry often implicitly assume that the working electrode surface is a uniform plane of activity and thus these measurements only provide average rates across an electrode surface. The effects of electrode surface heterogeneity on electrochemical behavior has been of long-standing interest [13–15] and the recent experimental work by Bond's and Oldham's groups have clearly demonstrated these effects on quasireversible dc and ac voltammetry [12]. The SECM, however, can provide direct and quantitative measurements of reaction–rate constants on micrometer-sized regions of electrodes and other surfaces [16–18]. Examples in which

ET rate constants are measured by SECM for a mediator at a heterogeneous surface include the hydrogen oxidation reaction on variable composition Pt catalyst [19] and several reactions on indium tin oxide and boron-doped diamond [20].

This work shows that the SECM can be used to image as well as locally measure rate constants at regions of differing ET kinetics present on GCE surfaces. Initial studies used direct-mode SECM to introduce artificial kinetic heterogeneities by local oxidation of micrometer-sized regions of a GCE [21]. In this study, the SECM is used to measure the heterogeneous ET rate for the Fe(II/III) couple at both the modified portions of the surface, as well as unmodified regions, which serve as a built-in control. This method is also applied to study kinetic heterogeneities at naturally occurring as well as intentionally introduced defects on GCEs.

Experimental

Reagents Iron(II) perchlorate hydrate was purchased from Aldrich Chemical (Milwaukee, WI, USA). All other chemicals were ACS reagent grade and used as received. Solutions were prepared from 18 MΩ cm ultrapure water (Milli-Q, Millipore, Bedford, MA, USA). All solutions were stored at room temperature and were not deoxygenated before use.

Electrodes The Hg/Hg_2SO_4 (MSE) reference electrode was manufactured in-house, and all potentials are reported versus this reference electrode. SECM tip electrodes were manufactured using 10 and 300 μm Pt wire from Goodfellow (Cambridge Science Park, UK) as described previously [22, 23]. The 3-mm diameter GCE used as a substrate was purchased from Bioanalytical Systems (West Lafayette, IN, USA). The 1-mm diameter GCE substrate was constructed from a carbon rod purchased from Alfa Aesar (Ward Hill, MA, USA) and was fabricated into a substrate electrode by potting the rod in EPON 828 epoxy (Miller-Stephenson, Danbury, CT, USA) with 13 wt.% triethylenetetramine hardener (Miller-Stephenson) and polishing to expose a disk. "Unoxidized" GCEs were prepared by polishing with an aqueous slurry of 0.05 μm alumina on cloth mounted on a polishing wheel rotating at 300 rpm. Subsequently, electrodes were rinsed with and sonicated in distilled–deionized water prior to use.

Experimental apparatus The SECM used in this work has been described previously [24]. The tip and substrate potentials are independently controlled versus a single reference electrode by a bipotentiostat (EI-400, Ensman Instruments, Bloomington, IN, USA). Tip movement is controlled by a micropositioning system that consists of three positioning motors (Burleigh, Fisher, NY, USA) driven by the Burleigh 6000 system controller. The positioning motors and translation stages are built into a single assembly and placed on a vibration isolation table (Newport, Irvine, CA, USA). A personal computer controls the tip positioning and data collection using software written in-house. The SECM cell consists of a small Teflon cup into which the substrate is placed, facing upwards, via a friction fit through a hole in the bottom of the cell.

Cyclic voltammetry experiments were conducted using the BAS 100B/W Electrochemical workstation (Bioanalytical Systems, West Lafayette, IN, USA). Background subtractions for cyclic voltammetric experiments were conducted by collecting nine voltammograms in the chosen electrolyte in the absence of electroactive species. These scans were averaged using the BAS software package and subtracted from voltammograms taken under identical conditions in the presence of the electroactive species of interest. The background signal in blank electrolyte often changed slightly in the first few scans and became more reproducible thereafter.

Generation of artificially introduced kinetic heterogeneities The generation of locally oxidized regions on GCE was performed as described previously [21]. A home-built current source [25] was used that allowed remote-controlled switching between potentiostatic and galvanostatic tip modes without disturbing the substrate potential or touching the electrodes. The SECM tip electrode was brought close to a larger GCE in a cell containing deionized water. A predetermined amount of current was then passed for a defined amount of time between the tip and substrate electrodes with the tip as the cathode and the substrate as the anode. This forced the reduction of solvent species at the tip electrode and the oxidation of the carbon surface in the region immediately under the tip.

Simulation of SECM current–distance curves with finite heterogeneous kinetics Software written to simulate the SECM current–distance response under conditions of finite heterogeneous electron transfer kinetics was generously supplied by Dr. Patrick Unwin. The program uses an alternating direction-implicit finite difference method to calculate the tip current at various distances, assuming finite heterogeneous ET kinetics at the substrate electrode and diffusion-limited kinetics at the tip [26].

Results and discussion

Figure 1 introduces a model of SECM under conditions of finite heterogeneous ET kinetics using the Fe(II/III) system

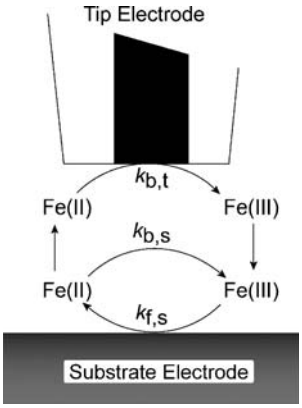

Fig. 1 A model of SECM with finite heterogeneous ET kinetics with the Fe(II/III) system

at a GCE. The terms k_f and k_b are the potential-dependent rate constants as described by the Butler–Volmer model:

$$k_f = k^0 \exp\left[-\alpha nF\left(E - E^{0'}\right)\Big/RT\right] \quad (1)$$

$$k_b = k^0 \exp\left[(1-\alpha)nF\left(E - E^{0'}\right)\Big/RT\right] \quad (2)$$

where k^0 is the standard heterogeneous ET rate constant, α is the transfer coefficient, n is the number of electrons involved in the reaction, F is the Faraday constant, R is the gas constant, T is the temperature, and $(E-E^{0\prime})$ is the overpotential. Subscripts s and t stand for processes occurring at the substrate and tip, respectively. In this work, we have assumed that (1) the ET process at the tip is mass-transport limited ($k_{b,t}\rightarrow\infty$) and (2) irreversible ET occurs at the substrate electrode (i.e., $k_{b,s}\rightarrow 0$). Condition 1 is met by holding the tip at high overpotentials for the oxidation of Fe(II) to Fe(III) and condition 2 holds due to the small k^0 for the Fe(II)/Fe(III) couple on unactivated GCEs [8, 23, 27]. Under these conditions, the ET rate constants are related to observable current by the classic current–potential equation [28].

Measurement of heterogeneous electron transfer rates by SECM Measurement of heterogeneous ET kinetics by SECM is similar to those previously described [26]. The measurement is made by collecting current–distance curves where the tip is first placed close to the substrate surface and current is monitored as the tip is slowly (typically 0.5 μm/s) moved away in a direction normal to the substrate surface. Collection of data while moving away from the surface avoided inadvertent collisions between the tip and substrate, which would damage the carbon surface and could change the ET parameters (see below). Current–distance curves are repeated at several substrate potentials to produce a range of rates at the substrate surface. The current–distance relationship for the limiting cases of $k_{f,s}\rightarrow\infty$ and $k_{f,s}=0$ are known as ideal positive and negative feedback behavior [29]. The region in which SECM kinetic measurement is possible lies between these two ideal cases where $k_{f,s}$ is finite.

The effect of varying $k_{f,s}$, through manipulation of the substrate potential on the shape of the current–distance curves, is demonstrated in Fig. 2, which shows a group of current–distance curves collected with a Pt tip at an unoxidized glassy carbon substrate in a solution of Fe(II) in 1 M H_2SO_4. The potential of the Pt tip is 0.80 V and the substrate potential varied from −1.0 to −0.2 V (vs. MSE). The data are plotted as normalized values of I_t vs. L where I_t is the ratio of the recorded tip current (i_t) over the diffusion-controlled limiting current at the tip $\left(i_{t,\infty}\right)$ and L is the tip–substrate separation (d) over tip electrode radius (a). Under these conditions, the high overpotential and rapid kinetics of Fe(II) oxidation at the Pt electrode (in 1 M H_2SO_4, E^0=−0.02 V vs. MSE, $k^0\sim 4\times10^{-3}$ cm s^{-1} at Pt [27]) produces a mass transfer limited reaction at the tip. In contrast, the sluggish kinetics for the reduction of tip-generated Fe(III) at the GCE allows the full range of kinetically controlled behavior to be observed. The data shows that, at more negative potentials (high $k_{f,s}$), the shape of the current–distance curve approaches (but does not meet) that of the ideal positive feedback response. At less negative potentials (low $k_{f,s}$), the shape of these curves approach that of the ideal negative feedback response. It is this change in the shape of the current–distance curves with applied potential that allows SECM to measure heterogeneous ET rates. Note that the small, periodic steps seen in the current–distance curves are artifacts caused by periodic adjustments by the positioning motor and are not related to the ET occurring at the substrate surface. Here and throughout, the tip–substrate position is initially determined

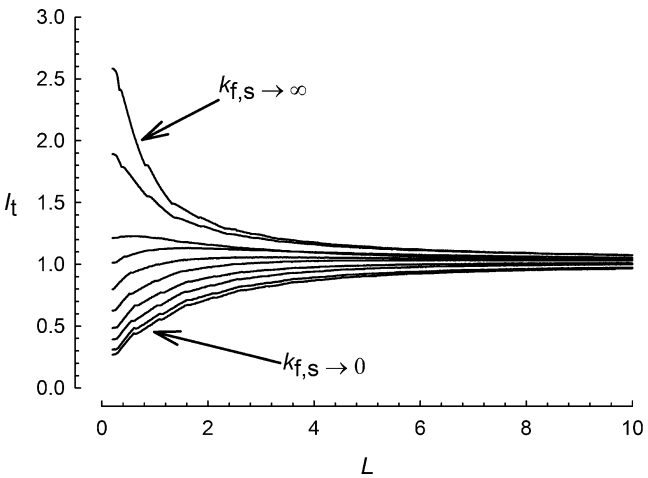

Fig. 2 SECM current–distance curves collected at various potentials with a 10-μm Pt tip electrode over an unoxidized GCE. Curves were collected in 2.0 mM $Fe(ClO_4)_2$ in 1 M H_2SO_4 with the tip biased at 0.8 V vs. MSE. The substrate potentials (from *top* to *bottom*) are −1010, −710, −560, −510, −460, −410, −360, −310, −260, and −210 mV

by setting the substrate potential to negative potentials (e.g., <−1.0 V) or more positive value (>−0.3 V) and using the theory for positive or negative feedback, respectively [29].

A selection of the curves from Fig. 2 are shown in Fig. 3—plotted as $\log_{10}L$—with the best-fit simulated current–distance data. Matching the simulated results gives normalized $K_{f,s}$ values ($K_{f,s}=k_{f,s}a/D$ where D is the diffusion coefficient of the mediator—4.08×10^{-6} cm^2 s^{-1} for Fe(III) in 1 M H_2SO_4, [27]) at each potential measured. I_T curves were simulated at intervals of $0.025\ln K_{f,s}$ allowing good identification of the experimental $K_{f,s}$ values by manual comparison of the experimental and simulated curves. Bracketing of the experimental data by the higher and lower simulated curves limits the error associated with determining $K_{f,s}$ to less than 6%.

Taking the log of Eq. 1 allows a "Tafel-type" plot of $\ln K_{f,s}$ vs. $(E_s-E^{0\prime})$ to be made based on Eq. (3):

$$\ln K_{f,s} = \ln k^0 a \Big/ D - \alpha n F \left(E_s - E^{0\prime}\right) \Big/ RT. \quad (3)$$

A linear regression of this plot yields α and k^0. Figure 4 shows a plot of $\ln K_{f,s}$ vs. applied potential for the curves in Fig. 3. A region of the plot shows the predicted linear dependence. Significant deviations from linearity occur at both small and large overpotentials. Data at high overpotential deviates from linearity because of limitations imposed by a finite mass transfer rate. At high overpotential, the current–distance response is approaching the ideal conductor regime where the tip current depends only on the tip to substrate spacing, and therefore, no kinetic information is available. Deviations from linearity at small overpotential can occur for two reasons. First, at small overpotential, there is a possibility that the reverse reaction is occurring at the substrate surface ($k_{b,s}$ is finite), which is

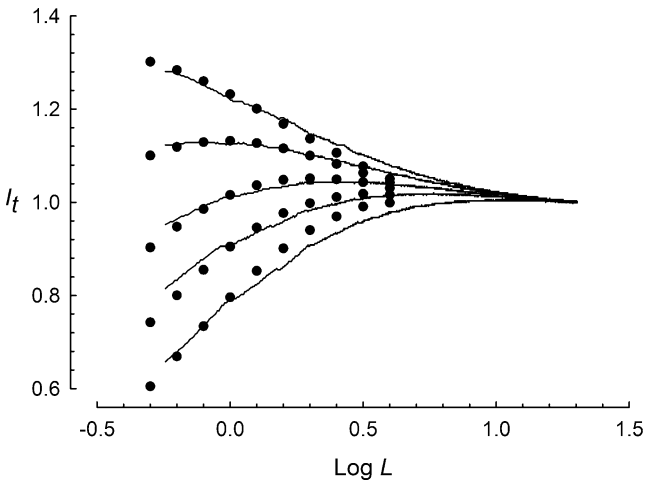

Fig. 3 A selection of SECM current–distance curves from Fig. 2 (*solid line*) shown with the best-fit simulation (*filled circle*) for each curve. The substrate potentials (from *top* to *bottom*) are −560, −510, −460, −410, and −360 mV vs. MSE

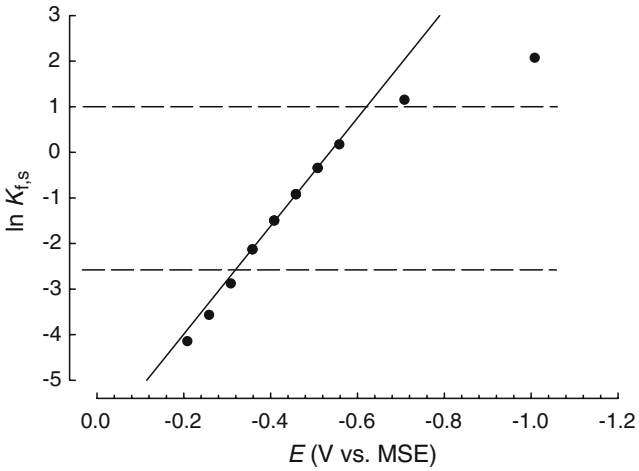

Fig. 4 Tafel plot of $\ln K_{f,s}$ vs. potential generated using the data from Fig. 3. The *dashed lines* indicate the range of $\ln K_{f,s}$ values accepted for linear regression analysis

not allowed in our model. This will lead to a decrease in tip current for the oxidation of Fe(II) since Fe(II) will also be consumed at the substrate. However, the slow kinetics for Fe(II) observed voltammetrically make this unlikely.

A second factor is the effect due to deviations from the ideal tip geometry. The case of slow kinetics at the substrate mimics the negative feedback response, which is defined by blocking diffusion of the mediator species to the electrode surface. The size of the insulating sheath around the conductive portion of the tip can profoundly affect the negative feedback response. When held close to an insulating substrate, a tip electrode with a large insulating sheath will be more effectively shielded from the mediator species than a tip with a very thin insulating sheath due to blocking of radial diffusion. The theoretical data generated as described above assumes a tip geometry with an RG value of ten where RG is a_{glass}/a_{tip}, the ratio of insulator sheath radius to the tip radius. Deviations from RG=10 will lead to either increased current at RG<10 or decreased current at RG>10. The tips used here had RG values of ~13 as measured by optical microscopy. The effect of nonideal tip geometry is illustrated in Fig. 3 where the bottom curve shown in Fig. 3 does not fit well to the theoretical response. More extreme deviations were observed as the potential of the substrate became increasingly positive. The low $k_{f,s}$ values lead to the deviation from linearity observed for the bottom three points in Fig. 4.

Linear regression data were only used for $\ln K_{f,s}$ values between 1 and −2.5 due to these known sources of nonlinearity in the Tafel plots. With these limits, the regression in Fig. 4 gives $k^0=1.66\times10^{-5}$ cm s^{-1} and $\alpha=0.305$ for this measurement at unoxidized carbon ($r^2=0.9994$). The α value is comparable to the value of 0.35 found from the rotating disk electrode data on polished and

oxidized GCE by Taylor and Humffray [27]. The k^0 value is typical of that measured by CV on *unoxidized* GCE, which ranges from 10^{-5} to 10^{-6} cm s^{-1} [23, 26, 27].

We repeated the rate constant measurement on various locations on the unoxidized, polished GCE and found the following k^0 values (in centimeters per second): $6.34\pm1.09\times10^{-5}$, $9.20\pm0.37\times10^{-5}$, $3.62\pm0.44\times10^{-5}$, and $1.20\pm0.33\times10^{-5}$. The standard deviations indicate three replicate measurements made at the same location. Each location shows a significant difference in rate constant and shows that the rate constant is highly variable on this surface—varying by up to sevenfold.

SECM kinetic measurements at artificially introduced active sites In a previous paper, we showed that the SECM tip could be used to make oxidized regions on glassy carbon by generating current densities of between 0.01 and 0.6 A cm^{-2} at a Pt disk electrode positioned about 1 μm from the GCE in 18 MΩ cm water [21]. Under these conditions—known as direct-mode oxidation—oxidized spots and patterns of tip dimension (typically one to three times the electrode diameter) could be formed on GCE surfaces. Figure 5 shows a background-subtracted cyclic voltammograms at a 1-mm diameter GCE in 7.6 mM $Fe(ClO_4)_2$ in 1 M H_2SO_4 before and after a direct-mode oxidation of 0.58 A cm^{-2} for 5 s was performed with a 300-μm Pt tip located in the center of the electrode. The voltammograms appear little different except for an increased current near 0 V at the oxidized electrode. Figure 6 shows Tafel plots generated from SECM kinetic measurements made over the oxidized region of the surface and an unoxidized region of the same surface. The data collected over the unoxidized region of the surface gives a $k^0=2.27\times10^{-5}$ cm s^{-1} and $\alpha=0.289$, while that collected over

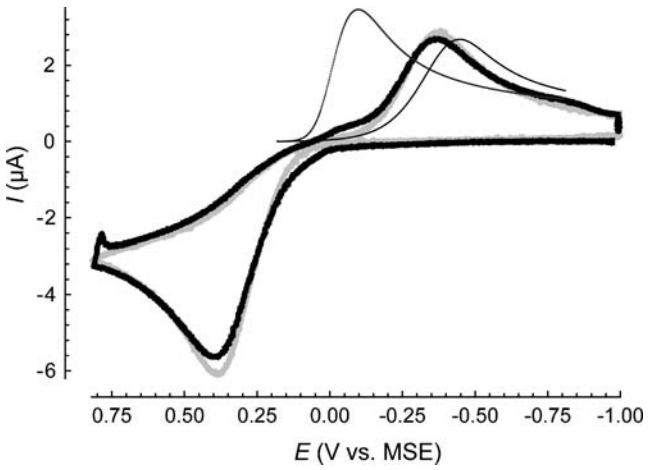

Fig. 5 Cyclic voltammograms for a 1-mm diameter GCE in 7.6 mM $Fe(ClO_4)_2$ in 1 M H_2SO_4 (*gray line*) before and (*thick black line*) after localized direct-mode SECM oxidation using a 300-μm diameter Pt tip. v=100 mV/s. Linear sweep voltammetry simulation of the Fe(III) reduction using the kinetic parameters measured in Fig. 6 for unoxidized carbon (*thin black line*) and oxidized carbon (*dotted line*)

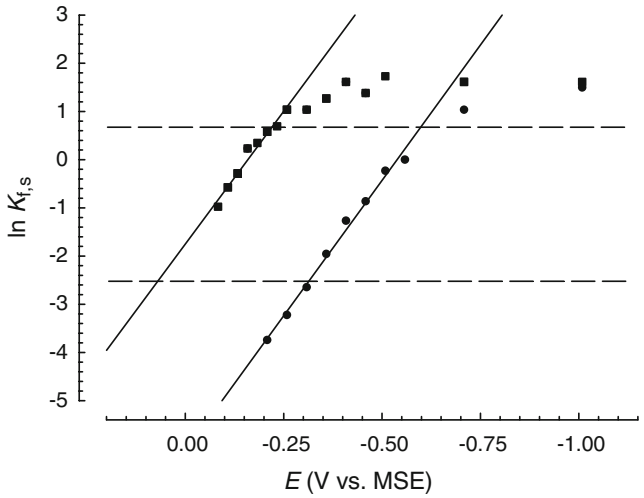

Fig. 6 Tafel plots for measurements made over oxidized (*filled squares*) and unoxidized (*filled circles*) regions of the same GCE described in Fig. 5. The *dashed lines* indicate the range of $\ln K_{f,s}$ values accepted for linear regression analysis

the oxidized spot gives a $k^0=1.67\times10^{-5}$ cm s^{-1} and $\alpha=0.283$. Good agreement is found in comparing this to Taylor and Humffray's result of $k^0=9.0\times10^{-4}$ cm s^{-1} at an oxidized GCE surface [27]. In comparing the CVs of Fig. 5, it is interesting to note that at an electrode that has nearly 10% of its surface area exhibiting an ET rate constant two orders of magnitude higher than the remainder was functionally identical to the completely unoxidized electrode. Such results indicate the care that must be taken in obtaining rate constants on possibly heterogeneous surfaces. The kinetic parameters found by SECM over the oxidized and unoxidized carbon regions were used as parameters in simulating linear sweep voltammograms for the reduction of Fe(III). These simulations are shown in Fig. 5. The peak for the oxidized carbon matches the increased current in the oxidized experimental CV and clearly shows the magnitude of the effect of oxidation on Fe(III) on oxidized carbon electrodes. The simulation of the unoxidized region matches the shape of the experimental peak but is shifted negative, indicating that the locally measured ET rate is apparently smaller than that observed in the CV. This is consistent with the spatial heterogeneity in rate constant noted above.

Although it would be possible to produce a complete kinetic map of an electrode surface by performing rate measurements over the entire two-dimensional grid, such measurements at present would be prohibitively lengthy. However, a sense of the power that such maps would present is given in Fig. 7 where the rate constant is measured as the tip is moved laterally across the substrate surface. Figure 7a shows line scans collected at a variety of substrate potentials by scanning the tip electrode over a region of carbon that had been oxidized using a 100-μm tip and applying a current of 0.58 A cm^{-2} for 5 s. The line scan

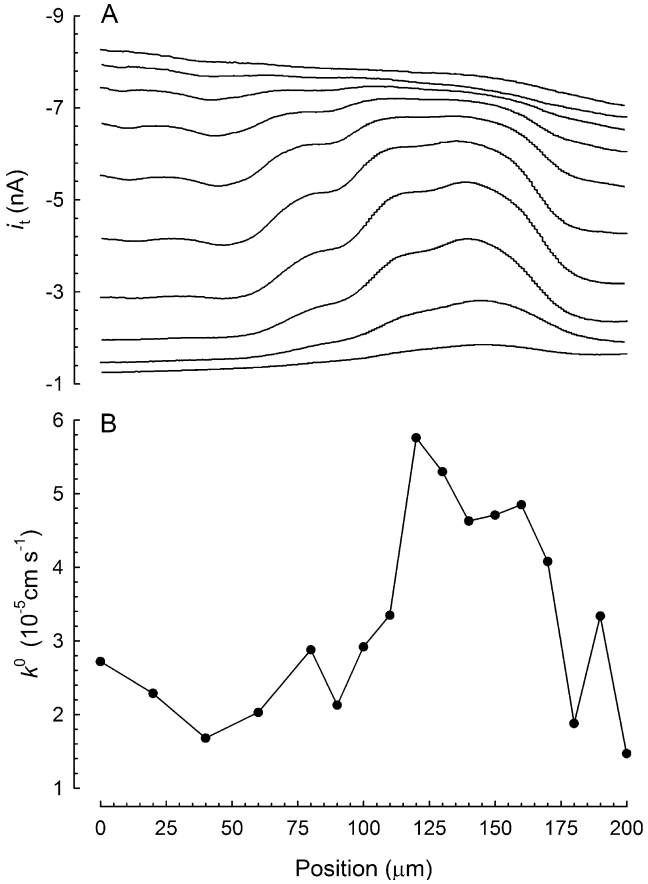

Fig. 7 **a** Data collected by scanning a 10-μm Pt tip across a 100-μm oxidized region at substrate potentials ranging from −1.0 V (*top line*) to −0.1 V (*bottom line*) vs. MSE. **b** k^0 values from SECM kinetic measurements at various sites across the same region as the line scan data

at the top was taken at a substrate potential of −1.0 V, which is near the diffusion-limited case. Note that the current trace is flat and slightly sloped, indicating no topographic features and a slight downward tilt in the substrate surface. The subsequent scans were collected at 100 mV intervals moving more positive. Note that as the potential is moved into a kinetically limited regime, a higher current region is observed, marking the oxidized portion of the surface. At the most positive potential, the rate of ET at both regions of the surface is essentially zero and an insulating response is observed; the residual positive slope again indicating a downward tilt. Figure 7b shows a series of SECM kinetic measurements made at various points across the same region of the surface as the line scans. As expected, the calculated rate constants over the oxidized region of the surface are consistently higher than at the unoxidized region of the surface. This data represents single measurements made at each site, but previous triplicate measurements showed about a 6% variance in the rates measured with this technique. The observed variation in the ET rate with distance and oxidation is consistent with the variation in ET rate noted above. The variation in rate in the oxidized zone likely reflects the underlying variability of the carbon substrate.

SECM kinetic measurements at small spots Experiments were conducted to see if the SECM rate measurement technique could be used to determine the heterogeneous ET rates at active sites on the surface of approximately the same size as that of the tip electrode. Small oxidized spots were formed on a 3-mm GCE using a 10-μm Pt tip at a current of 0.58 A cm^{-2} for 5 s. The same tip was also used to conduct the measurement. It was found that, with this combination of oxidized spot and tip size, the current–distance curves could not be fit to the theoretical data provided by the simulation. Figure 8 shows a typical current–distance curve that was collected at E_s=−0.3 V over the oxidized spot. Examination of the shape of the curve shows that the tip current initially decreases as the tip to substrate distance decreases. This indicates a slow rate of ET. However, as the distance continues to decrease, an increase in the tip current is observed. This behavior can be qualitatively explained by taking into account the relative area of the modified region of the surface compared to that of the electroactive region of the tip. Previous studies have shown that as the size of the substrate approaches that of the tip electrode, significant deviations from theory occur [26]. For this case, the area of influence for the tip electrode is considered to be a truncated cone with sides extending out from the edges of the electroactive region of the tip surface at 45° angles based on a random-walk model of diffusion. As the tip approaches the surface, the affected area of the substrate becomes smaller and smaller until it eventually reaches an area close to that of the tip itself. The shape of these current–distance curves can be rationalized

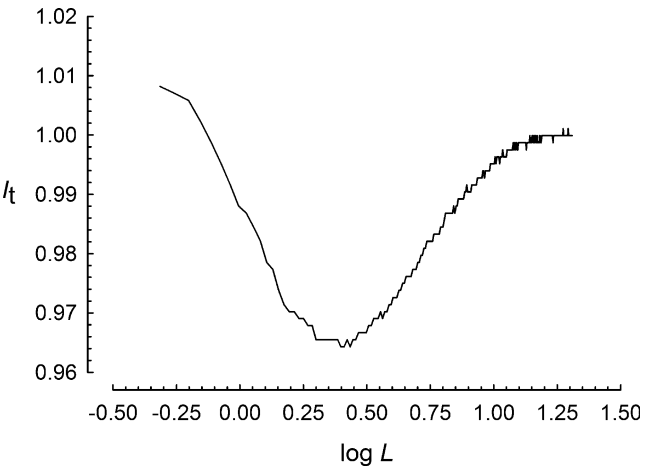

Fig. 8 SECM current–distance curve collected with a 10-μm Pt tip biased at 0.8 V vs. MSE over an approximately 10 μm oxidized region on a GCE surface biased at −0.3 V vs. MSE in a solution of 2 mM $Fe(ClO_4)_2$ in 1 M H_2SO_4

by taking into account the presence of the differing rates in a small region. At larger distances, the size of the affected area of the surface is larger than that of both the tip electrode and the modified region of the surface. The average rate across the affected area is thus different than either the modified or unmodified regions and, in this case, causes the tip to see a slower rate at the substrate surface and a decrease in tip current. As the tip to substrate distance decreases, the affected area of the substrate also decreases until it begins to approach that of the tip itself. At this point, more of the feedback process from the substrate is occurring at the oxidized spot than is occurring around the edges in the unoxidized regions. This leads to an overall increase in tip current at the smaller distances. In effect, the average rate varies with distance, making quantitative measurements unfeasible with the methods described in this study. If prior knowledge of the size and geometry of the target region is available, digital simulations should be able to provide quantitative results or, alternately, smaller tip electrodes could be used.

SECM kinetic measurements on damaged GCEs Experiments were conducted to examine kinetic differences occurring at intentionally added defect sites on GCEs. McCreery's group has shown that differences in carbon structure, namely, edge vs. basal plane, occur in and around defect sites on the carbon surface [7]. Experiments were attempted to observe this effect and quantitatively measure the differences by SECM. Figure 9 shows two SECM images collected over a region of carbon that was intentionally scratched with an SECM tip to produce surface defects. The scratching was accomplished by bringing a SECM tip into contact with and dragging it across the surface using the tip positioning motors. As discussed previously, imaging conditions can be manipulated to produce an image in which the contrast reflects either the topography of the electrode or the reaction–rate (i.e., reaction–rate imaging) [21]. This is seen in Fig. 9a, which is acquired at a substrate potential of −1.0 V, producing a positive feedback image. The lighter tones at the highest tip current are due to small tip–substrate separation. The image in Fig. 9b is collected at −0.4 V. At this potential, differences in ET rate become the primary contrast mechanism (reaction–rate image), although topography still plays some part. In general, the higher tip currents are due to higher ET rates. Due to the confounding effect of topography, images such as these cannot provide unequivocal identification of rate differences. Thus, current–distance measurements were made at three spots on the electrode surface to provide rate constant values. The locations of the three spots are labeled by the transparent rings in Fig. 9b and these correspond to the highest (whitest), lowest, and medium tip current locations. These three measurements, respectively, give $k^0=2.79\times10^{-5}$ cm s^{-1} and $\alpha=0.287$; $k^0=9.10\times10^{-6}$ cm s^{-1} and $\alpha=0.293$; and $k^0=1.86\times10^{-5}$ cm s^{-1} and $\alpha=0.287$. These indicate that a range of rates are found around defect-rich sites.

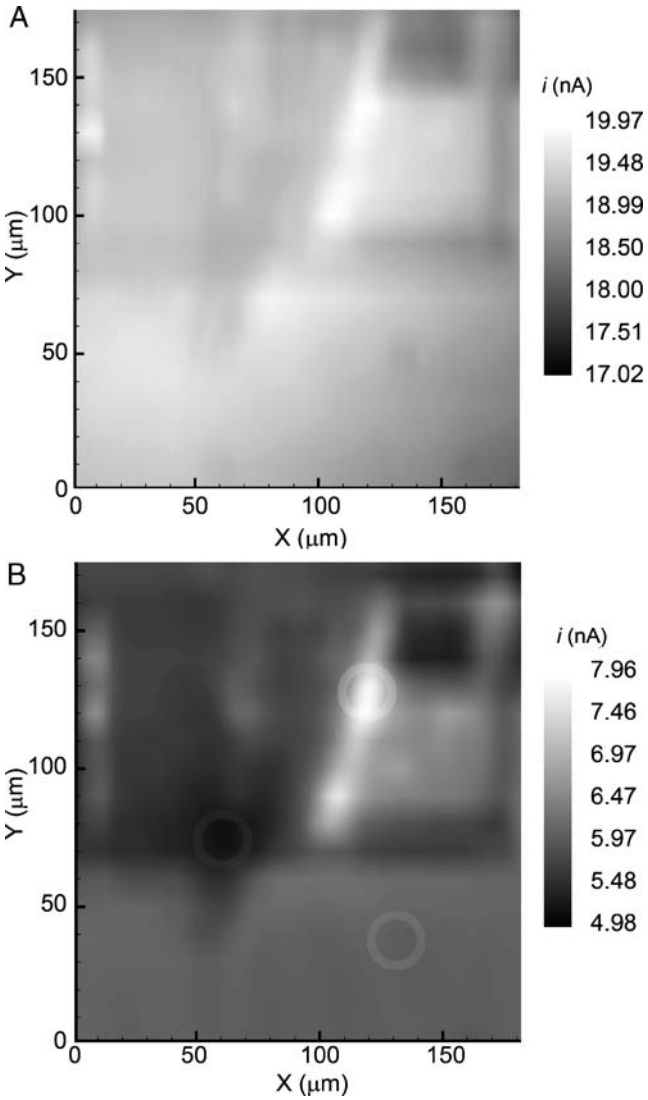

Fig. 9 SECM images of a defect-rich GCE surface collected with a 10-μm Pt tip biased at 0.8 V vs. MSE in a 2.0-mM solution of Fe $(ClO_4)_2$ in 1 M H_2SO_4. **a** Topographic image (substrate biased at −1.0 V) and **b** reaction–rate image (substrate biased at −0.4 V)

Conclusions

The Fe(II)/Fe(III) couple is highly sensitive to the state of the carbon electrode surface. This and the high spatial resolution of the SECM technique allow new views toward understanding the challenging surface properties of carbon electrodes. Direct quantitative measurements at micrometer-sized regions of an alumina-polished glassy carbon surface show that a surprising variation in k^0 exists—a small sample

of points showed greater than sevenfold spread in values. The measured values cluster around those measured with conventional cyclic and rotating disk voltammetry measurements. Production of locally oxidized regions of carbon surface indicate that the local regions of oxidized carbon have k^0 values two orders of magnitude higher than unoxidized GCE, similar to electrodes pretreated by bulk chemical or electrochemical oxidation. However, CV is unable to easily identify the presence of these oxidized regions even when they comprise nearly 10% of the surface area of an otherwise unoxidized electrode. Reaction–rate imaging with SECM produces images that show variation in ET rate across the surface; however, these images are often confounded by the presence of topographic information. Localized measurement of rate constant parameters can show the effect of topography and easily distinguishes topographic and kinetic effects. A limitation of this method is the requirement that the tip has a well-characterized geometry (in this study, an embedded disk in a finite insulator) and is smaller than the feature of interest. In particular, the relative size of spots that can be examined at various rates with a given tip size needs further examination and could be useful in defining the ultimate resolution of the reaction–rate imaging mode.

Acknowledgments The National Science Foundation (CHE-94144101) supported this work.

References

1. Kinoshita K (1988) Carbon: electrochemical and physiochemical properties. Wiley, New York, NY
2. McCreery RL (1991) In: Bard AJ (ed) Electroanalytical chemistry. Marcel Dekker, New York, pp 221–374
3. McCreery RL (2008) Chem Rev 108:2646–2687 doi:10.1021/cr068076m
4. Wu J, Pisula W, Mullen K (2007) Chem Rev 107:718–747 doi:10.1021/cr068010r
5. Jenkins GW, Kawamura K, Ban LL (1972) Proc R Soc Lond A Math Phys Sci 327:501–517 doi:10.1098/rspa.1972.0060
6. Jenkins GM, Kawamura K (1971) Nature 231:175 doi:10.1038/231175a0
7. Ray KG, McCreery RL (1997) Anal Chem 69:4680 doi:10.1021/ac9705531
8. McDermott CA, Kneten KR, McCreery RL (1993) J Electrochem Soc 140:2593–2599 doi:10.1149/1.2220868
9. Chen P, Fryling MA, McCreery RL (1995) Anal Chem 67:3115 doi:10.1021/ac00114a004
10. Engstrom RC, Johnson KW, DesJarlais S (1987) Anal Chem 59:670–673 doi:10.1021/ac00131a028
11. Bodalbhai L, Brajter-Toth A (1990) Anal Chim Acta 231:191 doi:10.1016/S0003-2670(00)86417-X
12. Lee C-Y, Guo S-X, Bond AM, Oldham KB (2008) J Electroanal Chem 615:1–11 doi:10.1016/j.jelechem.2007.11.029
13. Davies TJ, Moore RR, Banks CE, Compton RG (2005) J Solid State Electrochem 9:797 doi:10.1007/s10008-005-0699-x
14. Armstrong FA, Bond AM, Hill HAO, Psalti ISM, Zoski CG (1989) J Phys Chem 1989:6485 doi:10.1021/j100354a041
15. Lipkin SM, Cahen GL, Stoner GE, Scriber LL, Gileadi E (1988) J Electroanal Chem 135:368
16. Bard AJ, Mirkin MV (eds) (2001) Scanning electrochemical microscopy. Wiley, New York
17. Lu X, Wang Q, Liu X (2007) Anal Chim Acta 601:10–25 doi:10.1016/j.aca.2007.08.021
18. Wittstock G, Burchardt M, Pust SE, Shen Y, Zhao C (2007) Angew Chem Int Ed 46:1584–1617 doi:10.1002/anie.200602750
19. Jayaraman S, Hillier AC (2001) Langmuir 17:7857–7864 doi:10.1021/la010930b
20. Neufeld AK, O'Mullane AP (2006) J Solid State Electrochem 10:808–816 doi:10.1007/s10008-006-0180-5
21. Tenent RC, Wipf DO (2003) J Electrochem Soc 150:E131–E139 doi:10.1149/1.1538227
22. Wightman RM, Wipf DO (1989) In: Bard AJ (ed) Electroanalytical chemistry. Marcel Dekker, New York, pp 267–353
23. Wipf DO, Bard AJ (1991) J Electrochem Soc 138:469–474 doi:10.1149/1.2085612
24. Wipf DO (1994) Colloids Surf A 93:251–261 doi:10.1016/0927-7757(94)02872-9
25. Wipf DO (2003) In: Bard AJ, Wilson GS (eds) The encyclopedia of electrochemistry. vol. 3. Wiley-VCH, Weinheim
26. Bard AJ, Mirkin MV, Unwin PR, Wipf DO (1992) J Phys Chem 96:1861–1868 doi:10.1021/j100183a064
27. Taylor RJ, Humffray AA (1973) J Electroanal Chem 42:347–354 doi:10.1016/S0022-0728(73)80324-9
28. Bard AJ, Faulkner L (2001) Electrochemical methods. Wiley, New York
29. Bard AJ, Fan F-RF, Mirkin MV (1994) In: Bard AJ (ed) Electroanalytical chemistry. Marcel Dekker, New York, pp 243–373